MULTIPHASE LEVEL SET APPROACH TO LIDAR ROOF SEGMENTATION

KyoHyouk Kim and **Jie Shan**
Purdue University
School of Civil Engineering
550 Stadium Mall Drive
West Lafayette, IN 47907, USA
{kim458, jshan}@purdue.edu

ABSTRACT

This paper presents an approach to LiDAR point clouds segmentation for building roofs. Normal vectors determined from the original LiDAR point clouds are used as a homogeneous criterion representing planar roof planes. Segmentation is then performed iteratively by minimizing an energy function formulated as a multiphase level set framework. With multiphase level set formulation, up to n disjoint sub-regions can be segmented at a time by $\log_2 n$ level set functions. After convergence, each sub-region represented in 2D grid space shows the spatial extent of data points with the most similar normal vectors. Boundaries between different sub-regions correspond to roof ridges and those are represented as the union set of zero level sets of level set functions. In the final step, coplanar planes are separated into roof primitives by analyzing connectivity information. The main advantages of the proposed approach are 1) spatial extent of segmented roof planes is delineated in 2D grid space, and 2) this spatial extent provides more efficient way for determining topological relations among the segmented roof planes. To demonstrate our approach, segmentation results of a few buildings with different complexity are presented.

INTRODUCTION

For the past two decades, 3D building models have been considered as one of the most essential components for various applications such as 3D GIS, urban planning and telecommunication. For this reason, many researchers have reported different methods to reconstruct 3D building models with different data sources. LiDAR (**Li**ght **D**etection **A**nd **R**anging) is one of data sources used for this purpose. The main advantage of LiDAR is its capability to measure elevation at each observed data points with high accuracy, which makes it easier to detect buildings. With higher point density up to 10 points/m^2, detailed roof structures can also be reconstructed.

To reconstruct 3D building models from LiDAR data, a few successive steps have to be applied. First, non-ground points need to be separated from the original point clouds. This can be done by various methods such as morphological filtering (Zhang, Chen et al. 2003), height texture measures (Maas 1999; Bartels and Wei 2006) and labeling process (Shan and Sampath 2005). The identified non-ground points are then further refined by removing data points which are returned from non-building objects such as tress, cars, side walls of buildings and so on. This is accomplished by the first and last return analysis (Alharthy and Bethel 2002), eigen value analysis of covariance matrix (Shan and Sampath 2005; Verma, Kumar et al. 2006) and dimensionality learning (Wang and Shan 2009). In the subsequent step, building points are segmented into planar roof planes based on a certain similarity property. Finding planar roof planes is a key step toward 3D reconstruction of building models. This is usually accomplished through segmentation process. Fundamentally, there exist two different approaches. The 1st approach is to resample the original point clouds into grid data (Alharthy and Bethel 2002; Forlani, Nardinocchi et al. 2006). Then, various image processing algorithms are applied to this gridded data. The main advantage of this method is that it can reduce the complexity of the problem and increase the overall performance (Dorninger and Nothegger 2007). The main defect is that some artifacts may be induced during the resampling process, which leads to loss of the original data accuracy. The 2nd approach is to segment original point clouds directly. Therefore, original data accuracy can be maintained, but processing algorithm is more complex and it requires more processing time. The other difficulty in the 2nd approach is that it is not always easy to determine the topological relations among the segmented point clouds. To segment point clouds into planar roof planes, region growing, 3D Hough-transform and RANSAC (Random Sample Consensus) methods are generally applied. In the final step, polyhedral building models are reconstructed based on the topological relations among the segmented roof planes. To determine topological relations, roof topology graph (Verma, Kumar et al. 2006) and adjacent matrix (Sampath and Shan 2008) are

proposed. This paper mainly focuses on point clouds segmentation for building roofs. Our approach is based on the region based segmentation with multiphase level set theory. As the initial results of segmentation, segmented point clouds and the spatial extent of each segment are determined. Connectivity is then easily determined from the spatial extent of each segment.

PRINCIPLES

Multiphase Level Set Method

The original level set method is proposed by (Osher and Sethian 1988) as a numerical technique for tracking interfaces and shapes. The main idea is to embed a moving interface into a higher dimensional function, i.e. level set function. This method turns out to be very useful to represent shapes that change topology, e.g. breaking and merging as shown in figure 1.

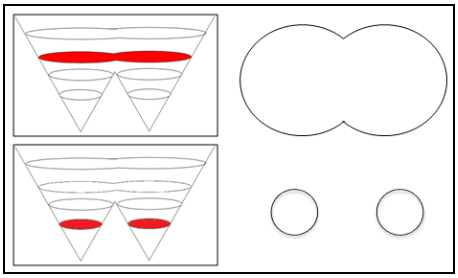

Figure 1. Topological changes represented by level set.

In computer vision, this level set method has been widely used for image segmentation and boundary detection problem. Let W be open and bounded subset in ¡ ^{2} and a curve C be the boundary of an open set w Î W, i.e. $C = \P w$ as shown in figure 2(left). In the level set, a curve C is represented implicitly as the zero level set of one higher continuous function f : W® ¡ . The function f is called level set function. Therefore, W is divided into two disjoint sub-regions based of the different of f, i.e. $f > 0$ and $f < 0$ as shown in figure 2.

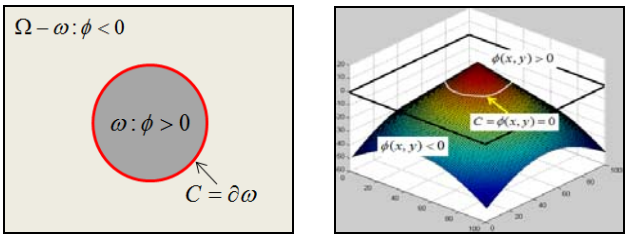

Figure 2. (Left) Implicit representation of a curve C, (right) level set function defined as a signed distance function.

(Osher and Sethian 1988) formulates the propagation of the evolving curve C as a PDE (Partial Differential Equation).

$$\frac{\P f(x,y,t)}{\P t} = F\,|\tilde{N} f\,| \quad \text{with } f(x,y,0) = f_0(x,y) \tag{1}$$

where t is evolving time, $f_0(x,y)$ is the initial level set function at $t = 0$ and F is speed for curve propagation. Therefore, the propagation of a curve in ¡ ^{2} is described by level set function f in ¡ ^{3} and the curve C always remains as the zero level set of f.

To apply level set method for image segmentation, the evolving curve needs to be stopped at the object boundary. For this purpose, two different approaches have been proposed. First, edge-stopping function is multiplied to the right side of equation (1). Edge-stopping function is defined as a nonnegative monotonically decreasing function such that it makes equation (1) vanish at the object boundary which has strong edge, i.e. high gradient. However, this approach may not work if the given image is very noisy or boundaries to be detected does not show high gradient. To overcome these defects, region based level set segmentation is proposed by (Chan and Vese 2001). In this approach, curve propagation is halted by energy minimization criterion rather than edge-stopping function. (Chan and Vese 2001) proposed the following equation as an energy function to be minimized.

$$E = m \times Length(C) + n \times Area(C_{in}) + l_1 \int_{C_{in}} |u_0 - c_1|^2 \, dxdy + l_2 \int_{C_{out}} |u_0 - c_2|^2 \, dxdy \tag{2}$$

where C is a curve, u_0 is an input image, $m \geq 0$, $n \geq 0$, l_1 and l_2 are fixed parameters, c_1 and c_2 are average intensity values inside and outside the curve C. The energy function of equation (2) is then minimized when the curve C lies on the object boundary because the last two fitting terms vanish. To rewrite equation (2) using level set, the Heaviside function $H(z)$ and delta function $d(z)$ are defined as equation (3).

$$H(z) = \begin{cases} 1 & \text{if } z \geq 0 \\ 0 & \text{if } z < 0 \end{cases}, \quad d(z) = H'(z) = \frac{d}{dz} H(z) \tag{3}$$

If we assume that level set function f has (+) and (-) values inside and outside the curve C, i.e. figure 2(right) corresponds to this case, length and area term in equation (2) can be rewritten as follows.

$$\begin{aligned} Area(C_{in}) &= \int_\Omega H(\phi(x,y)) dxdy \\ Length(C) &= \int_\Omega |\nabla H(\phi(x,y))| \, dxdy \\ &= \int_\Omega \delta(\phi(x,y)) |\nabla \phi(x,y)| \, dxdy \end{aligned} \tag{4}$$

In the same way, the last two fitting terms of equation (2) can also be rewritten using the level set function f. Combining equation (2)-(4), equation (2) is rewritten as a function of f as equation (5).

$$\begin{aligned} E = {} & m \int_\Omega d(f(x,y)) |\nabla H(f(x,y))| \, dxdy \\ & + n \int_\Omega H(f(x,y)) dxdy \\ & + l_1 \int_\Omega |u_0 - c_1|^2 H(f(x,y)) dxdy \\ & + l_2 \int_\Omega |u_0 - c_2|^2 (1 - H(f(x,y))) dxdy \end{aligned} \tag{5}$$

One level set function can only segment the given image u_0 into two sub-regions. To segment more sub-regions, multiphase level set method can be applied (Vese and Chan 2002). Allowing overlapping between level set functions, n disjoint sub-regions can be represented by $\log_2 n$ level set functions as shown in figure 3. Each sub-region is then represented by different signs of level set functions. For example, sub-region R01 shown in figure 3(left) is defined by the following condition: $f_1 < 0$ and $f_2 > 0$.

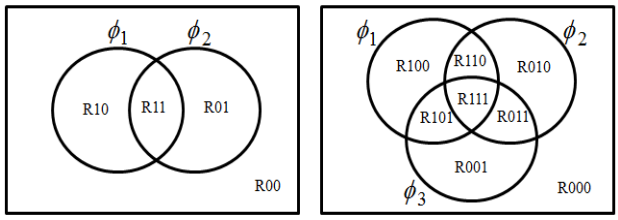

Figure 3. (Left) Four regions by two level set functions, (Right) eight regions by three level set functions.

Another extension of level set method is multichannel level set (Chan, Sandberg et al. 2000). This method allows more than one data layers to be involved for segmentation process. This can be used when the input image u_0 consists of multichannel data such as RGB or multispectral image. In the same manner as getting equation (5), energy function E can be formulated. For example, the energy function with two level set functions and three channels is then formulated as follows.

$$\begin{aligned} E = {} & l_1 \int_w \left(\frac{1}{3} \sum_{i=1}^{m=3} |u_{0,i} - c_{11,i}|^2 \right) H(f_1) H(f_2) dxdy \\ & + l_2 \int_w \left(\frac{1}{3} \sum_{i=1}^{m=3} |u_{0,i} - c_{10,i}|^2 \right) H(f_1)(1 - H(f_2)) dxdy \\ & + l_3 \int_w \left(\frac{1}{3} \sum_{i=1}^{m=3} |u_{0,i} - c_{01,i}|^2 \right) (1 - H(f_1)) H(f_2) dxdy \\ & + l_4 \int_w \left(\frac{1}{3} \sum_{i=1}^{m=3} |u_{0,i} - c_{00,i}|^2 \right) (1 - H(f_1))(1 - H(f_2)) dxdy \\ & + m_1 \times \int_w |\nabla H(f_1)| dxdy + m_2 \times \int_w |\nabla H(f_2)| \end{aligned} \tag{6}$$

where $m = 3$ is the number of channels, $u_{0,i}$ is the i-th channel of the input image u_0 and $c_{11,i}, c_{10,i}, c_{01,i}, c_{00,i}$ are average intensity values of the i-th channel of four regions. The last two terms are length regularization terms for the two level set functions. The energy function E of equation (6) should be minimized to find object boundary correctly. To minimize this function, corresponding Euler-Lagrange equation for each level set function is derived. Parameterizing the descent direction by an artificial time $t \geq 0$, the evolving equation can be derived. For example, evolving equation of $f_1(x, y, t)$ is represented as follows.

$$\begin{aligned} \frac{\partial f_1}{\partial t} = {} & \delta(f_1) \{ m_1 \times div\left(\frac{\nabla f_1}{|\nabla f_1|} \right) + \frac{1}{3} \sum_{i=1}^{m=3} \{ l_3 |u_{0,i} - c_{01,i}|^2 - l_1 |u_{0,i} - c_{11,i}|^2 \} H(f_1) \\ & - \frac{1}{3} \sum_{i=1}^{m=3} \{ l_2 |u_{0,i} - c_{10,i}|^2 - l_4 |u_{0,i} - c_{00,i}|^2 \} (1 - H(f_1)) \} \end{aligned} \tag{7}$$

where div is divergence operator. Equation (7) is then solved iteratively by applying the finite difference technique in the discrete domain.

SEGMENTATION

To find planar roof planes, we applied multiphase and multichannel level set segmentation. We aim to combine advantages from two different approaches presented in introduction, i.e. we do not resample the original point clouds and spatial extent of the segmented points is reflected in 2D grid space, which is represented as sub-regions of multiphase level set formulation. For this purpose, normal vectors determined from the original points clouds are used as a homogeneity criterion representing planar roof planes. The segmentation process is then to divide 2D grid

space enclosing all building points into disjoint sub-regions such that each one corresponds to one or a group of planar roof planes. We provide a detailed algorithm with two level set functions and three channels. In the end of this section, separation of coplanar planes into roof primitives is also discussed.

Normal Vector Calculation

To define any planer plane in $\mathbb{R}^3$, normal vector and distance from the coordinate origin are enough. Therefore, as the 1st step of segmentation, normal vector of each data point is to be estimated. Let $\boldsymbol{P}$ be the building points and $\boldsymbol{N}_i = (n_{x(i)}, n_{y(i)}, n_{z(i)})^T$ be the normal vector of the i[th] data point $\boldsymbol{p}_i \in \boldsymbol{P}$. $\boldsymbol{N}_i$ is usually determined from its neighboring points by local plane fitting. In this research, we used TIN (Triangular Irregular Network) structure to define the neighborhood of $\boldsymbol{p}_i$. $\boldsymbol{N}_i$ is then determined by averaging normal vectors of triangles incident to $\boldsymbol{p}_i$ as in equation (8).

$$\boldsymbol{N}_i = \frac{1}{n}\sum_{j=1}^{n} \boldsymbol{N}_{T_j} \tag{8}$$

where $\boldsymbol{N}_i$ is normal vector at $\boldsymbol{p}_i$, n is the number of triangles incident to $\boldsymbol{p}_i$, and $\boldsymbol{N}_{T_j}$ is the normal vector of the j[th] neighboring triangle. If the distance between $\boldsymbol{p}_i$ and one of two points of T_j is larger than two times the LiDAR ground spacing, normal vector of T_j is not included for the calculation of $\boldsymbol{N}_i$. If there are less than three triangles satisfying this condition, $\boldsymbol{p}_i$ is excluded for the subsequent process. Considering this is likely to produce more accurate normal vector in case $\boldsymbol{p}_i$ lies on the step edges or building boundaries as shown in figure 4.

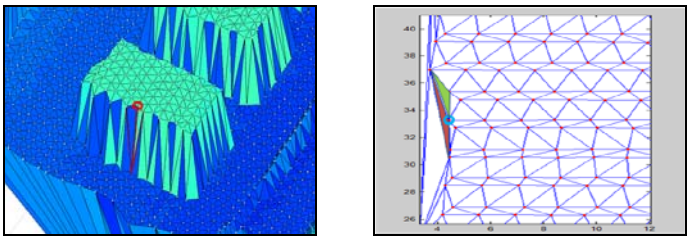

Figure 4. (Left) Points on the step edgs, (right) on the building boundary.

Once normal vectors of $\boldsymbol{P}$ are estimated, we analyzed the planarity of each data point. This can be achieved by PCA (Principal Component Analysis) or dimensionality analysis (Verma, Kumar et al. 2006; Sampath and Shan 2008). In this research, we analyzed the mean angle difference between $\boldsymbol{N}_i$ and $\boldsymbol{N}_{T_j}$ using the following equation.

$$\text{Mean Angle Difference} = \frac{1}{n}\sum_{j=1}^{n} \boldsymbol{N}_i \cdot \boldsymbol{N}_{T_j} \tag{9}$$

where (g) denotes the inner product of two vectors. If MAD of $\boldsymbol{p}_i$ is less than 15°, it is considered as a planar point. Otherwise the given point is excluded, i.e. non-planar point. One example of this process is shown in figure 5.

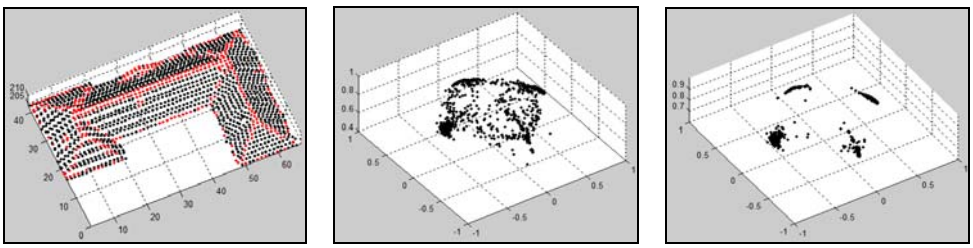

Figure 5. (Left) Plot of planr points (black dots) and non-planar points (red dots), (middle) plot of the unit normal vectors of all points, (right) plot of the unit normal vectors of planar points.

Formulation

Let $\boldsymbol{P}$ be planar points and $\boldsymbol{N} = (n_x, n_y, n_z)^{\mathrm{T}}$ be their normal vectors. We use $\boldsymbol{N}(1), \boldsymbol{N}(2)$ and $\boldsymbol{N}(3)$ to denote a vector consists of n_x, n_y and n_z components respectively. For the purpose of illustration, building points shown in figure 6(left) is used. First, we specify 2D grid space W with size M by N enclosing $\boldsymbol{P}$. The grid size depends on the average point density. One data point per cell is preferred. Two initial level set functions f_1 and f_2 are then determined as a signed distance function with the same size as W. Building boundary points are also determined by α-shape algorithm (Edelsbrunner, Kirkpatrick et al. 1983). Mask grid W_m is then defined using building boundary points, which is used to ignore any operation performed outside the building.

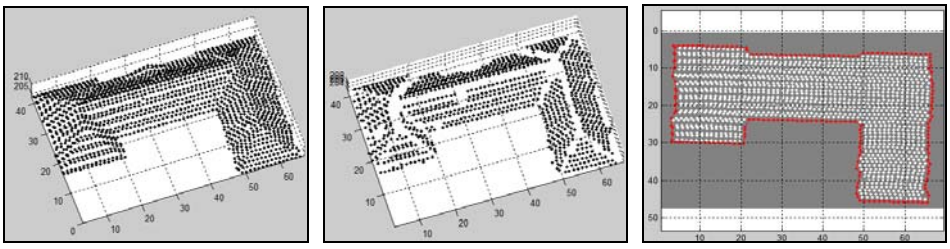

Figure 6. (Left) Building points, (middle) planar points, (right) W overlaid with boundary points (red dots).

To determine the energy function to be minimized, we follow the similar form presented in equation (6). The main difference is that four fitting terms are estimated from a set of normal vectors rather than an image. Therefore, the energy function can be formulated as equation (10).

$$
\begin{aligned}
E = {} & l_1 \int_{W_m} \frac{1}{3} \sum_{i=1}^{m=3} \left| \boldsymbol{N}(i) - \bar{\boldsymbol{N}}_{11}(i) \right|^2 H(f_1) H(f_2) \, dxdy \\
& + l_2 \int_{W_m} \frac{1}{3} \sum_{i=1}^{m=3} \left| \boldsymbol{N}(i) - \bar{\boldsymbol{N}}_{10}(i) \right|^2 H(f_1)(1 - H(f_2)) \, dxdy \\
& + l_3 \int_{W_m} \frac{1}{3} \sum_{i=1}^{m=3} \left| \boldsymbol{N}(i) - \bar{\boldsymbol{N}}_{01}(i) \right|^2 (1 - H(f_1)) H(f_2) \, dxdy \\
& + l_4 \int_{W_m} \frac{1}{3} \sum_{i=1}^{m=3} \left| \boldsymbol{N}(i) - \bar{\boldsymbol{N}}_{00}(i) \right|^2 (1 - H(f_1))(1 - H(f_2)) \, dxdy \\
& + m_1 \times \int_W |\nabla H(f_1)| \, dxdy + m_2 \times \int_W |\nabla H(f_2)| \, dxdy
\end{aligned}
\tag{10}
$$

where $\boldsymbol{N}(i)$ is a vector consists of the i$^{\text{th}}$ channel of $\boldsymbol{N}$, $\bar{\boldsymbol{N}}_{11}(i), \bar{\boldsymbol{N}}_{10}(i), \bar{\boldsymbol{N}}_{01}(i)$ and $\bar{\boldsymbol{N}}_{00}(i)$ are mean values of the i$^{\text{th}}$ channels of $\boldsymbol{N}$ for four sub-regions. Square bracket $[\,]_W$ represents M by N grid, i.e. the same dimension as W determined from a set of points inside the square bracket. Mean normal vectors of four regions are determined from data points whose horizontal locations are within the corresponding sub-regions. For example, $\bar{\boldsymbol{N}}_{10}$ is calculated as follows.

$$
\bar{\boldsymbol{N}}_{10} = \frac{1}{k} \sum_{i=1}^{k} \boldsymbol{N}_i \quad \text{, satisfying for all } i : f_1(\boldsymbol{p}_i(x,y)) > 0 \text{ and } f_2(\boldsymbol{p}_i(x,y)) < 0 \tag{11}
$$

where k is the number of points in sub-region R10 and $f_1(\boldsymbol{p}_i(x,y))$ and $f_1(\boldsymbol{p}_i(x,y))$ denote the evaluations of two level set functions at data point $\boldsymbol{p}_i(x,y)$. In the same manner as getting equation (7), we can derive evolving equations for f_1 and f_2. By applying the finite difference technique in the discrete domain, final evolving equation for f_1 is formulated as follows.

$$f_1^{n+1} = f_1^n + \Delta t \times d_0(f_1^n)\{ m_1 \times \left(\frac{\nabla f_1^n}{|\nabla f_1^n|} + \frac{1}{3}\sum_{i=1}^{m=3} \left[l_3 |N(i) - \bar{N}_{01}(i)|^2 - l_1 |N(i) - \bar{N}_{11}(i)|^2 \right] \right) H_e(f_1^n) \\ - \frac{1}{3}\sum_{i=1}^{m=3} \left[l_2 |N(i) - \bar{N}_{10}(i)|^2 - l_4 |N(i) - \bar{N}_{00}(i)|^2 \right] (1 - H_e(f_1^n)) \} \quad (12)$$

where f_1^n and f_1^{n+1} are the approximations of f_1 at time $(n)\Delta t$ and $(n+1)\Delta t$. $H_e(f_1^n)$ and $d_0(f_1^n)$ are regularized versions of the Heaviside and delta function. We refer the reader to (Rudin, Osher et al. 1992; Chan and Vese 2001; Vese and Chan 2002) for the regularization of the Heaviside, delta function and more detailed numerical algorithm. For the fixed parameters, we used the followings: $\Delta t = 0.01$, $m_1 = m_2 = 0.01 \times 255^2$ and $l_1 \sim l_4 = 1$. The evolving equation (12) is then iteratively minimized with initial level set functions. The following is a summary for these processes.

- Determine 2D grid Ω enclosing all building points with size M by N based on the average point density.
- Determine building boundary points and specify mask grid Ω_m.
- Initialize two level set functions f_{1_0} and f_{2_0} using a signed distance function.
- Repeat the followings until convergence or a given number of iterations.
  - Compute $H_e(f_1^n), d_0(f_1^n), H_e(f_2^n)$ and $d_0(f_2^n)$.
  - Compute $(f_1^n / |f_1^n|)$ and $(f_2^n / |f_2^n|)$.
  - Compute mean normal vectors of four regions.
  - Update new approximation f_1^{n+1} using equation (12).
  - Check convergence.

In figure 7, intermediate plots of segmentation process are presented. Point clouds of four sub-regions are shown in different colors. The changes of spatial extent for four sub-regions are also presented in figure 8. The union of two zero level sets of level set functions are also shown in figure 8(right) as white lines.

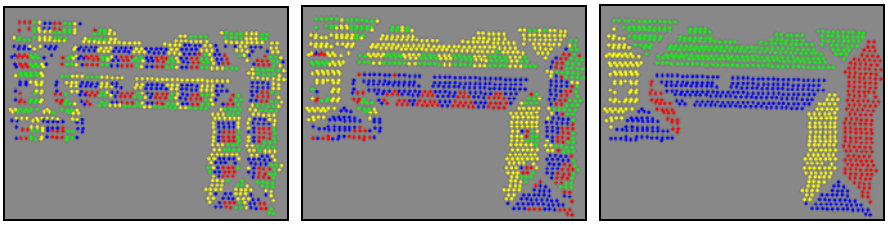

Figure 7. Plots of segmented point clouds: (Left) 1th iteration, (middle) 4th iteration, (right) 8th iteration.

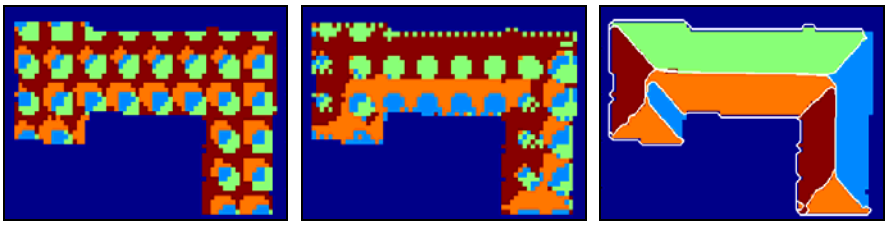

Figure 8. Spatial extent of four sub-regions: (Left) 1th iteration, (middle) 4th iteration, (right) 8th iteration.

As we can see from figure 7 and 8, the iteration process converges to the global minimum at the 8th iteration step. The initial 2D grid space Ω is divided into four sub-regions, each of which represents a group of planar roof planes with the most similar normal vectors. In figure 9, we present each sub-region $\Omega_{(i)}$ separately. This representation is from the definition of sub-regions with multiphase level set formulation. For example, sub-region R11 is represented by $\{\Omega_{(1)}(x,y) : H_e(f_1)H_e(f_2)\}$. It can be seen that each sub-region consists of a few coplanar

planes, which are a group of planes with the same normal vectors, but are spatially separated. Separating these coplanar planes into roof primitives is preferred to determine the topological relations and reconstruct 3D roof model. To separate these planes, we applied a four-connectivity analysis (Haralick and Shapiro 1992) to each sub-region shown in figure 9. In figure 10, the final results after plane separation are presented. Each separated sub-region is represented with different colors and each one matches well with one roof primitive. The separated point clouds are also shown in figure 10(right). Two more segmentation results with different buildings are also presented in figure 11.

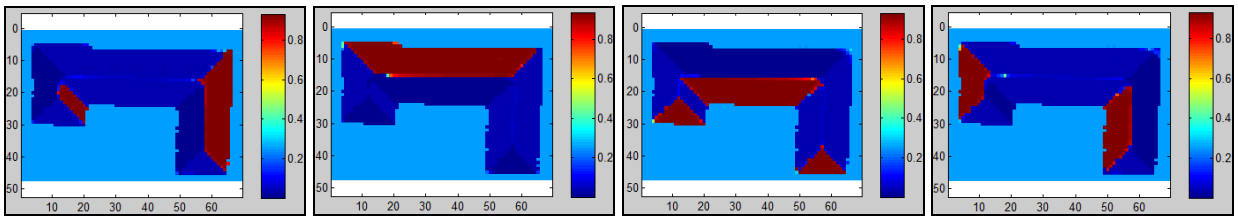

Figure 9. Representation of four sub-regions: (From left to right) $W_{(1)}$ = R11, $W_{(2)}$ = R10, $W_{(3)}$ = R01, $W_{(4)}$ = R00.

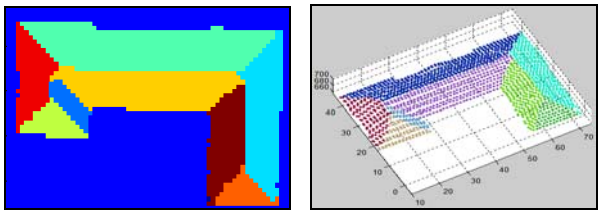

Figure 10. Final separation results: (Left) Separated sub-regions $\bar{W}_{(i)}$ and (right) separated point clouds.

Initial Results

In this paper, we applied two level set functions to segment four sub-regions. As the results, segmented point clouds for roof primitives and their spatial extent in 2D grid space are derived. In this process, we need to discuss how to determine the number of level set functions. Theoretically, any number of level set functions can be used and formulating corresponding energy function is straightforward with some complexity. For example, building data shown in the 1st row of figure 11 consists of five groups of planar roof planes. The segmentation result shown is derived by applying three level set functions, i.e. up to eight sub-regions can be segmented. The problem may arise when we apply only two level set functions to this data. Intuitively, we can guess some of sub-regions may consist of roof planes, which have different normal vectors. This problem may be resolved by applying recursive segmentation. Once all sub-regions are separated, we can determine if each separated sub-region consist of one roof primitive. If not, further segmentation is applied to the corresponding separated sub-region with proper feature vector.

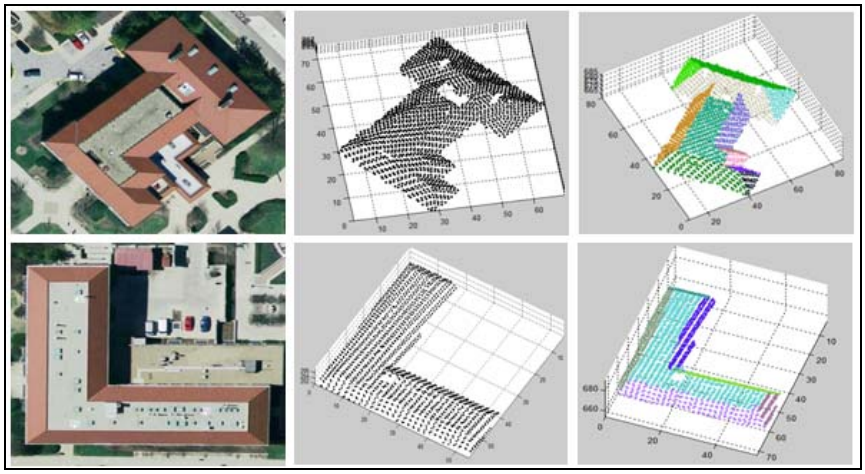

Figure 11. More segmentation results.

CONCLUSIONS

We presented a new approach to point clouds segmentation. To keep the original data accuracy, normal vectors determined from the original point clouds are used as input feature vectors. Segmentation is then performed iteratively by minimizing the energy function formulated as multiphase level set framework. Once the iteration process converges to the global minimum, each sub-region represents either one roof primitive or a group of roof planes with the same normal vectors. Roof primitives are then easily separated by analyzing the connectivity of each segment. To demonstrate our approach, two and three level set functions are tested with different building data points. In the future research, complete algorithm for reconstructing 3D roof models based on the results presented in this paper will be exploited. Recursive segmentation algorithm and more intensive tests with different data set will be carried out.

REFERENCES

Alharthy, A. and J. Bethel, 2002. Heuristic Filtering and 3D Feature Extraction from LIDAR Data, *IAPRS International Archives of Photogrammetry and Remote Sensing and Spatial Information Sciences*, **34**(3/A): 29-34.

Bartels, M. and H. Wei, 2006. Segmentation of LIDAR Data Using Measures of Distribution, *International Archives of Photogrammetry, Remote Sensing and Spatial Information Sciences*, **36**(7): 426~31.

Chan, T. F., B. Y. Sandberg, et al., 2000. Active contours without edges for vector-valued images, *Journal of Visual Communication and Image Representation*, **11**(2): 130-141.

Chan, T. F. and L. A. Vese, 2001. Active contours without edges, *IEEE Transactions on Image Processing*, **10**(2): 266-277.

Dorninger, P. and C. Nothegger, 2007. 3D segmentation of unstructured point clouds for building modelling, *International Archives of the Photogrammetry, Remote Sensing and Spatial Information Sciences*, **35**(3/W49A): 191?96.

Edelsbrunner, H., D. Kirkpatrick, et al., 1983. On the shape of a set of points in the plane, *IEEE Transactions on Information Theory*, **29**(4): 551-559.

Forlani, G., C. Nardinocchi, et al., 2006. Complete classification of raw LIDAR data and 3D reconstruction of buildings, *Pattern Analysis & Applications*, **8**(4): 357-374.

Haralick, R. M. and L. G. Shapiro, 1992. *Computer and Robot Vision*, Addison-Wesley Longman Publishing Co., Inc. Boston, MA, USA.

Maas, H. G., 1999. The potential of height texture measures for the segmentation of airborne laserscanner data, 4th Ariborne Remote Sensing Conference and Exhibition, Ontario, Canada.

Osher, S. and J. A. Sethian, 1988. Fronts propagating with curvature dependent speed: algorithms based on Hamilton-Jacobi formulations, *Journal of Computational Physics*, 12-49.

Rudin, L., S. Osher, et al., 1992. Nonlinear total variation based noise removal algorithms, *Physica D*, **60**(1-4): 259-268.

Sampath, A. and J. Shan, 2008. Building roof segmentation and reconstruction from LiDAR point clouds using clustering techniques, *IAPRS International Archives of Photogrammetry and Remote Sensing and Spatial Information Sciences*, **37**(B3a): 279-284.

Shan, J. and A. Sampath, 2005. Urban DEM generation from raw lidar data: A labeling algorithm and its performance, *Photogrammetric Engineering & Remote Sensing*, **71**(2): 217-226.

Verma, V., R. Kumar, et al., 2006. 3D building and modeling from aerial LIDAR data, IEEE Computer Society Conference on Computer Vision and Pattern Recognition (CVPR'06).

Vese, L. A. and T. F. Chan, 2002. A multiphase level set framework for image segmentation using the Mumford and Shah model, *International Journal of Computer Vision*, **50**(3): 271-293.

Wang, J. and J. Shan, 2009. Segmentation of LiDAR point clouds for building extraction, ASPRS 2009 Annual Converence, Baltimore, Maryland.

Zhang, K., S. C. Chen, et al., 2003. A progressive morphological filter for removing nonground measurements from airborne LIDAR data, *IEEE Transactions on Remote Sensing and Geoscience*, **41**(4): 872-882.